Remote Inspection of wind turbine blades using UAV with photogrammetry payload

D. Zhang, K. Burnham, L. Mcdonald, C. Macleod, G. Dobie, R. Summan and G. Pierce
University of Strathclyde
Glasgow, G1 1RD, UK
dayi.zhang@strath.ac.uk

Abstract

Visual Inspection is regularly used as a method of non-destructive testing (NDT) to find defects in large component structures. Wind turbine blades, regularly located in isolated environments, are typically difficult to access. In order to reduce operational and maintenance costs and extend asset lifetime, a project for the remote inspection of blades to accurately assess surface integrity is being undertaken. The remote inspection solution combines an unmanned aerial vehicle (UAV) with a photogrammetry payload to provide visual reconstruction of a blade for a holistic condition overview. Photogrammetric software is used to process the captured images to generate a 3D blade profile. A waypoint guidance algorithm controls the UAV to complete a full blade surface capture at constant distance, minimising motion blur. The results provide an accurate 3D reconstruction of the used blade complete with defects, discontinuities and markings and hence visual inspection using UAV combined with photogrammetry has been successfully implemented.

1. Introduction

Visual Inspection is regularly used as a method of non-destructive testing (NDT) to find defects in large component structures. Remote inspection of blades can reduce operational and maintenance costs and extend the asset lifecycle. Wind turbine blades, regularly installed on the top of the tower, are typically difficult to access. An Unmanned Aerial Vehicle (UAV) is a pilotless flying vehicle which provides flexibilities to undertake many challenging access problems. In the literature, UAVs have been utilised in many visual inspection fields, such as wall and roofs [1,2], power lines [3] and underground pipelines [4]. The current state-of-art of the UAV inspection of wind turbines focus on the algorithms to detect the defects from offline pictures [5] and path planning for the contact inspection [6,7]. Such approaches do not provide results with the position and location information, which is useful for credible and meaningful surface condition evaluation.
3D photogrammetry reconstruction is a technology whereby 2D images are used to generate a textured 3D model, providing an intuitive overview of the test object. The

An accepted author manuscript of the following research output: ZHANG, D., Burnham, K. C., McDonald, L., MacLeod, C. N., Dobie, G., Summan, R., & Pierce, S. (2017). Remote inspection of wind turbine blades using UAV with photogrammetry payload. 56th Annual British Conference of Non-Destructive Testing - NDT 2017, Telford, United Kingdom.

reconstructed model contains the approximate image locations, which allows the inspector to easily assess the condition of the testing object with the complex geometry. The reconstruction has been used in many fields, such as museum artefacts digitisation [8], UAV indoor navigation [9] and nuclear tank inspection [10]. The reconstruction can be accomplished by some commercial software, such as Autodesk Recap and Agisoft Photoscan. Researchers also developed the algorithms to achieve the reconstructions such as real scale [11] and 3D builds based on a single image [12].

To ensure the camera, with its limited field of view covers most of the blade, the UAV must follow a scan trajectory and as such a controller system is designed and applied. Linear and nonlinear controllers are two formats of UAV controllers implemented in literature. State of the art nonlinear controllers have demonstrated fast-moving stability and robustness with low uncertainties [13-15]. Proportional-Integral–Derivative (PID) controller is a type of linear controller and has been applied on the UAV in different forms [16,17]. Although the PID controller is less robust and not suitable for the fast speed control, it is easier to implement and is still able to stabilise the UAV under slow moving speed [18]. Considering the laboratory environments and the task requirements, the PID controller is selected to be implement in this project.

This paper has the following structure: Section 2 describes the UAV control, including the methodology, controller design and result discussions. The methodology and result discussions of the photogrammetry reconstruction are presented in Section 3.

2. UAV Control

2.1 Methodology

The UAV utilised (AscTec Firefly) [19] has a payload capacity of 600g and a twenty-minute battery life, shown in Figure 1. It contains six rotors and can generate 36N thrust in total [19]. The UAV has an on-board Core2 DUO computer (pre-installed Linux Operating System) to execute the applications for serial devices such as a camera.

Figure 1. AscTec UAV Top View

The camera installed on the UAV is Point Grey machine vision camera CM3-U3-50S5C-CS [20] with 8mm, F2.4, 57.8° FOV (field of view) lens [21] and captures 4 Mega Pixels (MP) raw images at 2Hz. To reduce the motion blur, the shutter time was changed from 60ms (factory settings) to 30ms. In addition, six external 135W 5500k lights were set-up at suitable locations around the blade to increase the light intensity and make it more representative of an outdoor inspection. Figure 2 depicts the captured images, with 60ms

shutter time, 30ms shutter time with and without lights. The captured images are saved to the hard drive on the UAV on-board computer and exported to the laptop after the inspection scheme has completed.

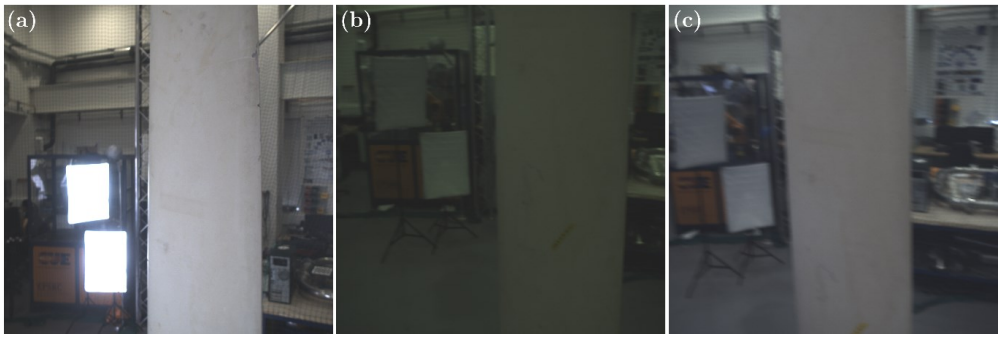

Figure 2. UAV captured images under (a)30ms shutter with lights (b)30ms shutter without lights (c)60ms shutter without lights

The inspection object is a part of a Gaia–Wind wind turbine blade [22], with observable cracks and dust on the surface. The blade is 3.1m height, 386mm wide on the top and 619mm on the button.

To achieve the autonomous UAV control, the path of the UAV is produced based on the UAV poses related to the inspection object. The path provides the reference guidance trajectory to feed the UAV controller for appropriate control actions. Due to the geometry of the blade is prior unknown and irregular, the path is a smooth circular trajectory to maintain the UAV with certain distances to the centre of the object. Comparing with the descending, the UAV takes longer to stabilize at a pose after climbing. Therefore, the UAV starts circular manoeuvring around the blade at 3.1m height and finishes at 0.7m height. The flying path contains nine circles with certain distances to the blade centre in different altitudes. It takes about 40 seconds to finish one circular manoeuvring. Because of the geometry of the blade, the radius of the top circle is 1100mm and the rest of the circles are increased 50mm progressively.

Considering the performance of the controller, the circular trajectory is digitized to many waypoints. The controller guides the UAV to a certain waypoint stably. Once the UAV reached the waypoint, the controller assigns the next waypoint. Cogitating the UAV speed, camera overleaping and the pose of the blade, the step between each waypoint is 150mm in translations; 45 degrees in yaw angle, giving eight points per circle.

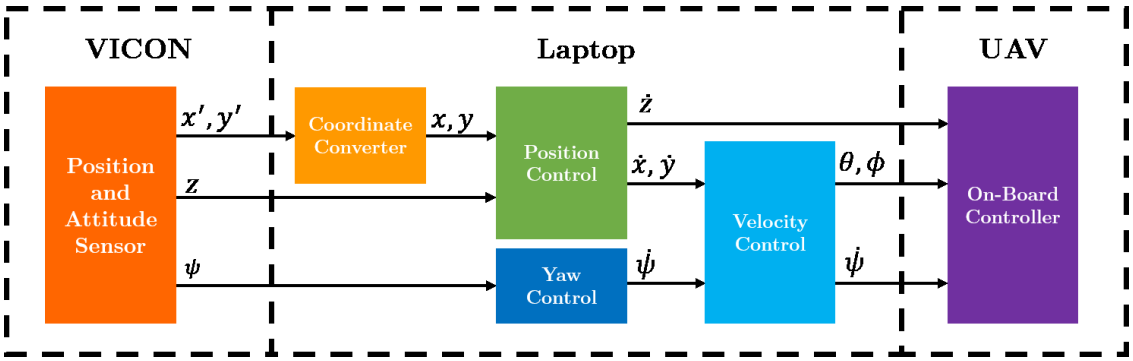

Figure 3. High-level architecture of the UAV system

The control system, shows in Figure 3, is used in this project. It contains three layers: VICON, Laptop and UAV. The VICON MX motion capture system [23] is an optical based 6 Degree of Freedom (D.O.F.) pose tracking system, working as an indoor navigation replacement of IMU (Inertial Measurement Unit) and GPS (Global Positioning System) measurement systems. It measures the UAV positions and attitudes, blade centre position and transfers this to a laptop on TCP/IP protocol in 100Hz. The system utilised featured twelve cameras and has approximately 8 x 7 x 7m coverage volume. The asymmetric combination of seven reflectors on the top of the UAV is defined as a unique object in VICON system, shown in Figure 3. Reflectors for the VICON object were placed on the bottom of blade to allow the system to determine the centre position of the blade.
The (x,y) position from VICON is converted from the global to UAV coordinate on the laptop. The converted (x,y) position, altitude and yaw information are passed to the controllers in the laptop, which calculate control commands for the UAV on-board controller. The communication between the laptop and UAV is established by XBee modules as the manufacturer defaults [24]. On-board controller then turns the incoming commands to the rotor speeds to accomplish the required UAV actions. The average control rate is around 20Hz, which is limited by the wireless communication throughput and UAV on-board processing speed.

2.2 Controller Design

For a typical UAV, the combination of torques, generated from the rotors, produces the attitude angles and vertical lift. Pitch and roll angles are coupled with the forward and lateral accelerations. The lift from the propellers produces the acceleration in the vertical direction. When the UAV is hovering in a pose, the accelerations and velocities are approximate to zero. When the UAV is assigned to a new pose, the appropriate accelerations and velocities are calculated and executed. The control system, shown in Figure 4, is implemented by PID (Proportional-Integral–Derivative) closed-loop controller.

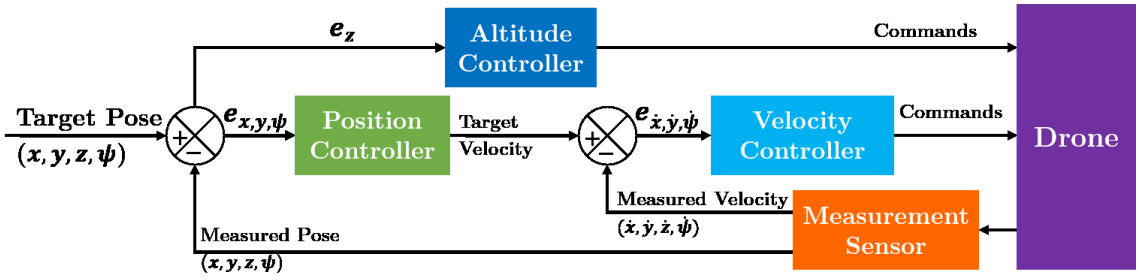

Figure 4. UAV position and attitude control system

PID controller uses the feedback system to continuously calculate the error between the measured value and setpoint. The output of the controller is the sum of the scale (P term), integration (I term) and changing rate (D term) of the error. The system characteristic is affected by the three terms, which can be tuned by altering k_p, k_i and k_d. The parameters of each PID term of controllers used in this project is listed in Table 1.

Table 1. Parameters of PID term in the controllers.

	k_p	k_i	k_d
Altitude PID	7	0	1.1
x position PID	1.5	0	1.2
y position PID	1.5	0	1
Yaw angle PID	35	0.001	0
x velocity PID	1	0.005	0.1
y velocity PID	1	0.002	0.1
Yaw rotation rate PID	1	0	0

The control system includes two subsystems, where x, y, ψ(yaw) are implemented by three cascade multi-loop controllers (System 1) and a parallel single PID controller (System 2) for the vertical position.

System 1 contains three independent controllers for each x, y, ψ(yaw) variable, implemented by the multi-loop structure, where the PID controller in first loop calculates the desired velocities from the error between measurement and target poses for the second layer controller. The errors of the velocities are the input of the second loop, which the output is the attitude commands for the UAV on-board controller. The speed controller of yaw has been implemented by the Asctec. Therefore, the second loop in yaw controller only includes the proportional term and designed as a speed limiter.

System 2 is applied by a single PID closed-feedback-loop because the vertical velocity controller has been included in the UAV's on-board controller. The error of altitude is the input of the System 2, which creates the vertical velocity updates to the on-board controller.

2.3 Experimental Results and Discussion

The trajectory errors are useful to estimate the stability and performance of the UAV. In this paper, the main part of the UAV flying path is nine circles around the blade. The nine circles have different height levels and different radius. Therefore, the trajectory errors are focused on the error and standard deviation of radius and height, detailed in Table 2.

The results show the mean error of the height increased with the altitude decreased. Similarly, the mean error of the radius slightly rose when the altitude descended.

Unlike the mean errors, the changes of standard deviation do not have a strong relationship to the altitudes. Therefore, the stabilities of UAV are quite similar in each altitude level. However, the standard deviations of height position are approximately four times larger than the standard deviations of the radius, which indicates the UAV had larger drifts in the Z direction.

Table 2. Mean error and standard deviation of radius and height in different altitude (mm)

Nominal Radius	Nominal Height	Mean Radius Error	Mean Height Error	Standard Deviation (Radius)	Standard Deviation (Height)
1100	3100	5.02	4.51	11.73	40.05
1150	2800	17.83	7.97	8.80	29.40
1200	2500	17.07	5.99	10.00	37.21
1250	2200	17.37	3.46	12.44	38.30
1250	1900	13.46	8.81	10.09	41.89
1250	1600	10.14	3.97	14.11	38.82
1250	1300	17.97	19.65	10.91	42.87
1250	1000	13.15	14.26	13.02	42.24
1250	700	12.94	24.94	12.88	37.97

Figure 5 shows the plot of radius and altitude errors in the whole flying scheme. Excluding the take-off and landing progress, the peak-to-peak errors are -56mm and 129mm in radius and altitude respectively. The figure shows the UAV is less stable in height position than the radius, which supports the claims from the Table 2. The errors during the landing progress were changing dramatically, which is related to the fast speed landing and noisy altitude sensor.

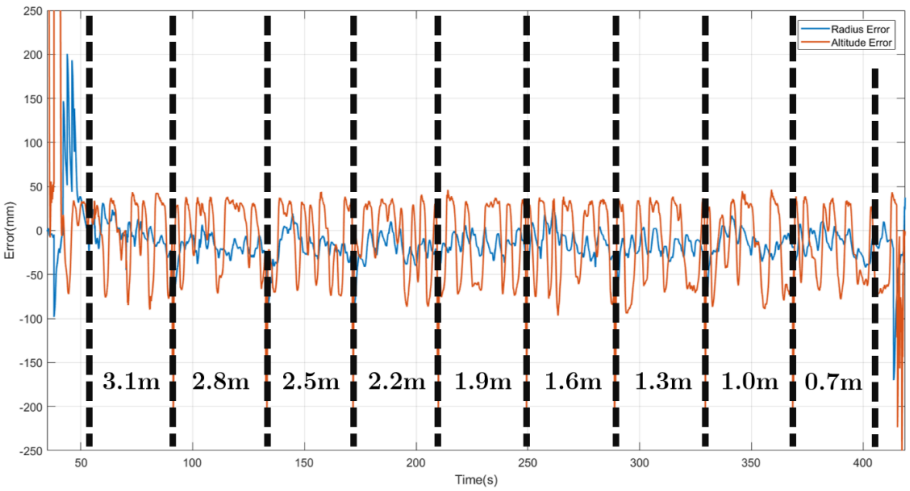

Figure 5. UAV radius and altitude errors

The UAV control is mainly based on the linear PID controller, who's the performance depends on tuning parameters (k_p, k_i and k_d). For example, the standard deviation, indicates the UAV stability, can be reduced by further tuned Proportional parameter. The Integral parameter of PID controller can be adjusted for the faster response and reducing the mean error of trajectory.

In addition, the speed in the Z direction (height) is controlled by the Asctec built-in controller, which used the pressure sensor to provide altitude measurement. The pressure sensor has much lower accuracy than the VICON system. The height can be stabilised by building a customised vertical speed controller in the laptop and bypassing the Asctec built-in controller.

Moreover, the communication between the UAV and the laptop is built on the XBee protocol, which limits throughput (57.6kbps) and control frequency (~20Hz). Therefore, the wireless communication protocol introduced the latency between the laptop and UAV

actions, which contributed part of the error. To reduce the latency, XBee can be replaced by the higher throughput protocol, such as Wi-Fi.
Furthermore, the controller can be replaced by the nonlinear controller, such as backstepping to further reduce the error and improve the stability.

3. Photogrammetry Reconstruction

3.1 Methodology

The photogrammetry reconstruction is achieved by the Agisoft Photoscan [25], a commercially available stand-alone software product which performs photogrammetric processing of digital images and generates 3D spatial data. Around 600 images are captured during the UAV inspection, includes time during the take-off and landing. The raw images were saved on the UAV on-board computer, then copied to the laptop for the further processing.
Though the dusts and cracks are visible on the surface, to better quantize the performance of the 3D reconstruction and adjust the camera focusing, the blade surface was prepared prior to the scanning. Ten 6.5mm dots and a 20mm textured yellow tape were pasted on the surface. The camera lens was manually adjusted for optimum focusing.
The software assumes the images are captured from a series of cameras in various position. Therefore, the background environment provides the reference points for the reconstruction. Firstly, the software aligns the photos to calculate the estimated position of the images, followed by the camera positions optimisation. Then, the point cloud, mesh and texture are built to create more detailed 3D objects. The final textured 3D model, achieved by the software, is shown in Figure 6.

Figure 6. Agisoft Reconstructed Model

To ascertain the accuracy of a visual reconstruction of the blade, the reference CAD model is captured by the GOM ATOS Triple Scan system. The system uses the narrowband blue light technology, permits precise measurement independent of

environment noises and produces high accuracy measurement with the error less than 20µm [26]. The mesh data from the Agisoft software was imported into GOM Inspect software for comparison with the 3D reference model. Because the photogrammetry is a dimensionless technique and the scale factor is unknown during the reconstruction, the output from the software does not contain the actual size information of the model. Therefore, prior to comparing the models, a scaling factor for the mesh and the coordinates allocation were firstly required. These were achieved by identifying two distinctive points from the mesh and fine-tuned by minimizing the surface difference. The GOM Inspection software returned a prealignment error factor and deviation map for the model comparison.

3.2 Experimental Results and Discussion

The reconstructed mesh, built from AscTec UAV images by Agisoft software is shown in Figure 6. Figure 7 shows the comparison between textures from the original images and the reconstructed mesh. The images indicate the dots and texture on the blade surface are clearly identified in the reconstructed model. In addition, discontinues on the blade leading edge is recognisable from the reconstructed mesh, shown in Figure 8.

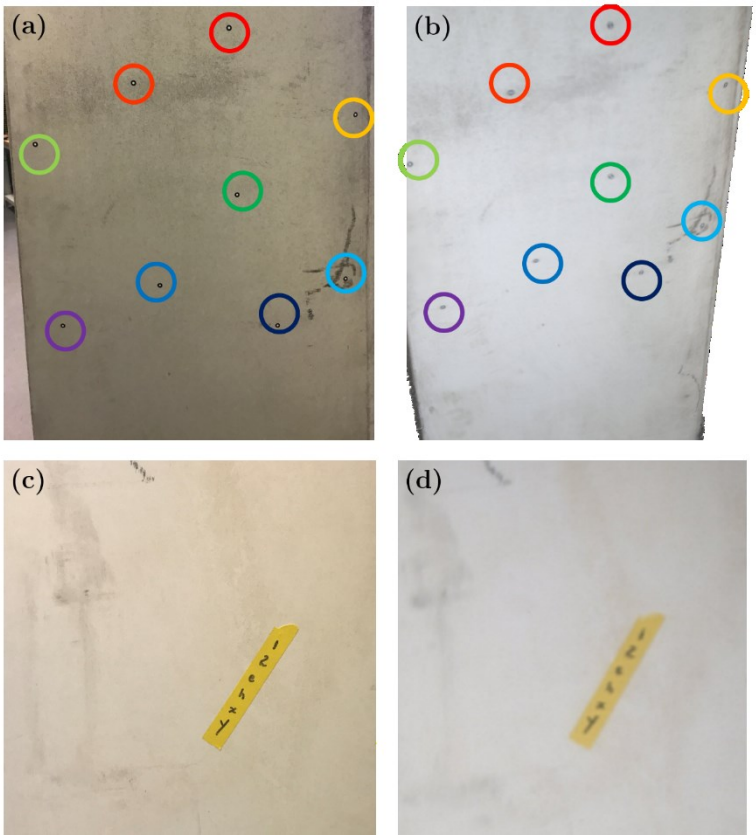

Figure 7. Comparison between the phone photo and reconstructed model (a)(c) Reference Camera captured, (b)(d) reconstructed mesh

Figure 8. Defect shows on the reconstructed mesh

Then, the mesh was imported into the GOM Inspect software for quantized comparison with the reference model of the blade. Besides, to quantize the effects from the light intensity as mentioned in Section 3 the experiment was undertaken in the three light conditions: 30ms shutter with external light supply, 30ms shutter without external light and 60ms shutter without external light. Results, shown in Figure 9, are the deviation maps from GOM software comparison report. The deviation values of the top half of the blade are listed in Table 3.

Deviation results show the 30ms shutter with the external light has the best reconstruction result and 30ms shutter without light has the worst result.

Table 3. standard deviations of reconstructed model in different light conditions

	30ms shutter With light	30ms shutter Without light	60ms shutter Without light
Prealignment Deviation(mm)	1.36	2.43	2.31

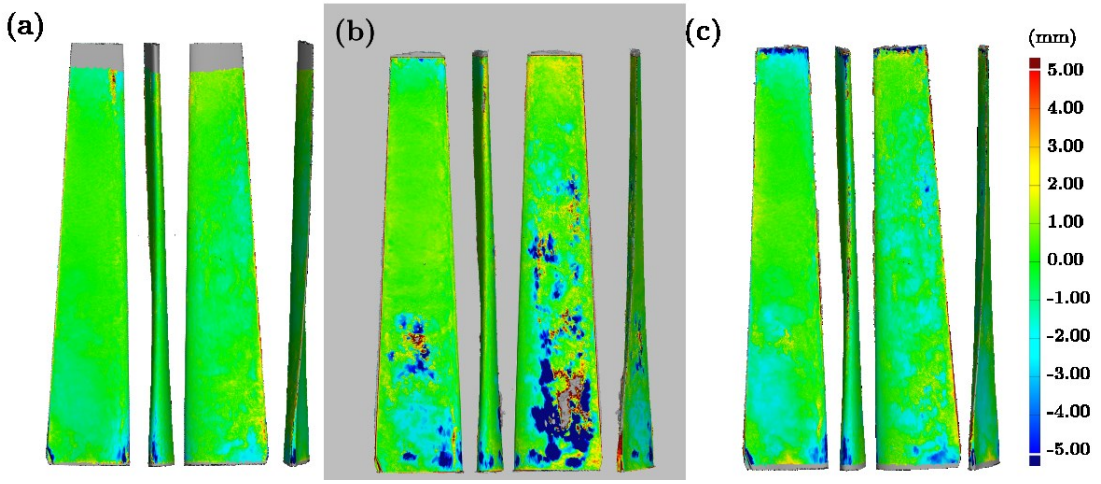

Figure 9. Deviation maps of the reconstructed model captured in different light intensity (a) 30ms shutter with light (b)30ms shutter without light (c) 60ms shutter without light

The experiment results illustrate the light intensity and motion blur affect the reconstruction performance. The images captured under low light intensity are not bright enough to allow the software to distinguish the blade. Motion blur destroyed the image information and the image is not able to use for the reconstruction. However, decreasing shutter time can reduce the blur and sacrifice the brightness at the same time. Hence, the light intensity and shutter time can be further optimised to achieve the better result.
Additionally, the reconstruction models in this paper were built from the raw images. The post-processed images, such as adjusting the brightness and contrast, might be able to provide the better reconstructed result. The UAV flying path and flying stability relate to the model quality. Due to the circular trajectory and non-circular geometry, the distance between the camera and blade surface are not constant and the camera focuses were not kept on the blade surface. Better trajectory planning or distance measurement sensor might be able to improve the reconstructed result.

4. Conclusions

This paper presented the implementation of the remote photogrammetric wind turbine testing with the UAV. The inspection scheme is achieved by the UAV following the circular trajectory. The UAV autonomous flight, including take-off and landing, is guided by the linear PID controller, which is relatively simple and easy to implement. The software has successfully reconstructed the 3D wind turbine model based on the images from the UAV camera. The details of blade surface can be observed from the textured model. The experiments were repeated under 30ms, 60ms shutter time and different light conditions to manage the experiments close to an outdoor inspection.
The results show that the remote photogrammetric inspection of the wind turbine blade is achievable. The overview condition and defects are recognisable from the non-destructive point of view.

References

1. Kestrel-Cam. Aerial building inspection and survey. url: http://kestrel-cam.co.uk /aerial-building-inspection/.
2. flyingeyeuk. Building Inspection - Aerial Building/Historic Surveys. url: http:// flyingeyeuk.com/services/surveys-and-inspections.html.
3. Jingjing Zhang et al. “High Speed Automatic Power Line Detection and Tracking for a UAV-Based nspection”. In: 2012 International Conference on Industrial Control and Electronics Engineering (2012).
4. Vertex Air. UAV Thermal Imaging. url: http://vertexaccess.co.uk/vertexair/services/thermal-imaging/.
5. Long Wang and Zijun Zhang. “Automatic Detection of Wind Turbine Blade Surface Cracks Based on UAV taken Images”. In: IEEE Transactions on Industrial Electronics (2017). doi: 10.1109/tie.2017.2682037.
6. Sungwook Jung et al. “Mechanism and system design of MAV(Micro Aerial Vehicle)-type wall-climbing robot for inspection of wind blades and non-flat surfaces”. In: 2015 15th International Conference on Control, Automation and Systems (ICCAS) (2015). doi: 10.1109/iccas.2015.7364634.
7. Martin Stokkeland, Kristian Klausen, and Tor A. Johansen. “Autonomous visual navigation of Unmanned Aerial Vehicle for wind turbine inspection”. In: 2015

International Conference on Unmanned Aircraft Systems (ICUAS) (2015). doi: 10.1109/icuas.2015.7152389.
8. Mohammad Nabil and Fathi Saleh. “3D reconstruction from images for museum artefacts: A comparative study”. In: 2014 International Conference on Virtual Systems & Multimedia (VSMM) (2014). doi: 10.1109/vsmm.2014.7136681.
9. Slawomir Grzonka, Giorgio Grisetti, and Wolfram Burgard. “A Fully Autonomous Indoor Quadrotor”. In: IEEE Transactions on Robotics 28.1 (2012), pp. 90–100. doi: 10.1109/tro.2011.2162999.
10. Ruaridh A. Clark et al. “Autonomous and scalable control for remote inspection with multiple aerial vehicles”. In: Robotics and Autonomous Systems 87 (2017), pp. 258–268. doi: 10.1016/j.robot.2016.10.012.
11. H. Navarro et al. “Fuzzy Integral Imaging Camera Calibration for Real Scale 3D Reconstructions”. In: Journal of Display Technology 10.7 (2014), pp. 601–608. doi: 10.1109/jdt.2014.2312236.
12. A. Saxena, Min Sun, and A.y. Ng. “Make3D: Learning 3D Scene Structure from a Single Still Image”. In: IEEE Transactions on Pattern Analysis and Machine Intelligence 31.5 (2009), pp. 824–840. doi: 10.1109/tpami.2008.132.
13. Yimeng Tang and Ron J Patton. “Phase modulation of robust variable structure control for nonlinear aircraft”. In: Proceedings of 2012 UKACC International Conference on Control (2012). doi: 10.1109/control.2012.6334625.
14. Filiberto Mu˜noz et al. “Second order sliding mode controllers for altitude control of a quadrotor UAS: Realtime implementation in outdoor environments”. In: Neurocomputing 233 (2017), pp. 61–71. doi: 10.1016/j.neucom.2016.08.111.
15. Zhenyue Jia et al. “Integral backstepping sliding mode control for quadrotor helicopter under external uncertain disturbances”. In: Aerospace Science and Technology 68 (2017), pp. 299–307. doi: 10.1016/j.ast.2017. 05.022.
16. S. Bouabdallah, P. Murrieri, and R. Siegwart. “Design and control of an indoor micro quadrotor”. In: IEEE International Conference on Robotics and Automation, 2004. Proceedings. ICRA 04. 2004 (2004). doi: 10.1109/robot.2004.1302409.
17. E. Altug, J.p. Ostrowski, and C.j. Taylor. “Quadrotor control using dual camera visual feedback”. In: 2003 IEEE International Conference on Robotics and Automation (Cat. No.03CH37422) (). doi: 10.1109/robot.2003.1242264.
18. Gabriel Ho_mann, Steven Waslander, and Claire J Tomlin. “Quadrotor Helicopter Trajectory Tracking Control”. In: (Aug. 2008).
19. AscTec. Asctec Firefly. url: http://wiki.asctec.de/display/AR/AscTec+Firefly.
20. FILR. Chameleon3 5.0 MP Color USB3 Vision (Sony IMX264). url: https: //www.ptgrey.com/chameleon3-50-mp-color-usb3-vision-sony-imx264-2.
21. Computar. M0824-MPW2. url: https://computar.com/product/1331/.
22. Gaia-Wind. Gaia-Wind. url: http://www.gaia-wind.com/.
23. VICON. VICON MX System. url: https://www.vicon.com/.
24. AscTec. XBee Modules. url: http://wiki.asctec.de/display/AR/XBee+Modules.
25. Agisoft. Agisoft Photoscan. url: http://www.agisoft.com/.
26. GOM. ATOS Triple Scan - Revolutionary scanning technique. url: http://www.gom.com/metrology-systems/atos/atos-triple-scan.html.